Robust Topographical Representation for Longitudinal Propagation of Tau Pathology

Jiaxin Yue[1,2], Jianwei Zhang[1,2], Xinkai Wang[1,2], and Yonggang Shi[1,2](✉)

[1] Stevens Neuroimaging and Informatics Institute, Keck School of Medicine, University of Southern California (USC), Los Angeles, CA 90033, USA
[2] Ming Hsieh Department of Electrical and Computer Engineering, Viterbi School of Engineering, University of Southern California (USC), Los Angeles, CA 90089, USA
yshi@loni.usc.edu

Abstract. Tau pathology is a hallmark of Alzheimer's disease (AD), and longitudinal tau positron emission tomography (PET) provides valuable insights into disease progression. However, the integration of tau PET data into computational models remains limited by challenges in encoding topographical information and ensuring longitudinal consistency. Existing biomarker-based representations often lack spatial flexibility and fail to account for covariance between brain regions. Additionally, traditional approaches often treat longitudinal scans as independent observations, neglecting temporal coherence. To address these limitations, we propose a novel Multiresolutional Reeb Graph representation that encodes the spatiotemporal propagation of tau topographical information. Our method constructs Reeb graphs to capture tau topography at a static time point and extends them into a multiresolutional framework to model disease evolution. We introduce a topology-based measurement for quantifying pathology spatial distribution similarity, and a severity interleaving distance for robust longitudinal staging. The efficiency of the proposed representation is validated in two downstream tasks: an integrated subtyping and staging system, and the longitudinal pathology prediction. The promising results compared with the current methods demonstrate the great potential of the proposed representation to enhancing the application of longitudinal tau PET data, and offering a reliable approach for studying AD progression.

Keywords: Tau pathology · Longitudinal · Topology.

1 Introduction

Tau is a hallmark pathology of Alzheimer's disease (AD)[8], and its accumulation has strong correlation with AD symptoms. It can be quantified spatially in the brain using positron emission tomography (PET), enabling the study of disease progression *in-vivo* and even pre-symptomatically [18]. Previous research has demonstrated that the topographical information of tau PET is effective in staging AD [4][9] and predicting future neurodegeneration [14]. The emerging of large-scale longitudinal tau PET data provides even greater opportunities for

the development and validation of predictive models. However, integrating longitudinal tau PET data into existing computational methods remains challenging due to the lack of valid representations, which further compromises the robustness of longitudinal analyses. Therefore, establishing a reliable topographical representation is crucial for effectively incorporating tau PET data into current learning-based frameworks.

The application of longitudinal tau PET data currently faces two major challenges. Firstly, the topographic information is not effectively encoded in biomarkers derived from tau PET imaging. In most studies, tau PET data is only used as a scalar biomarker for disease staging [10][8]. While some advanced analyses [20][9] incorporated the spatial distributions of tau accumulation, they remain constrained by the limited biomarkers and rigid region-of-interest (ROI) definitions based on the established atlases. These biomarker-based representations lack topographical flexibility, that ignoring the inter-regional covariance and longitudinal coherence in tau progression. The second challenge is the accurate longitudinal measurements of accumulation [3]. Measurement uncertainty, biological variability, and other confounding factors complicate the assessment of true variation in protein accumulation. Moreover, most longitudinal tau PET scans are analyzed as independent static observations, while the intrinsic temporal coherency is ignored or underestimated as a simple linear process [19], limiting the ability to capture complex disease dynamics. Therefore, a topography-specific representation that enables a spatiotemporal characterization of longitudinal tau pathology propagation is essential for improving the analysis and interpretation of longitudinal tau PET data.

To overcome these limitations, we propose a topographical representation to effectively handle the longitudinal tau PET data. Firstly, we adopt a topographical representation based on Reeb graph analysis [22], which was originally proposed for characterizing the spatial distribution of tau pathology in cross-sectional data and identifying its subtypes. This topographical representation is then extended into a Multiresolutional Reeb Graphs (MRGs) framework for encoding the temporal propagation. The MRGs representation is adaptive to the focal distributions of tau accumulations, and the transitions across resolutions robustly characterize the dynamic pathology progression. Secondly, based on the topology and properties of MRGs, a topology similarity is proposed for quantify the spatial similarity of tau accumulations, and a temporal severity measurement is proposed for robust staging.

We apply the proposed MRGs representation to longitudinal tau PET imaging data from the Alzheimer's Disease Neuroimaging Initiative (ADNI) [11]. Two downstream tasks are conducted for validating the efficiency of the representation. In the first experiment, we modified the community detection algorithm originally used for the cross-sectional clustering problem [22] into a multi-stage framework for integrating subtyping and staging within a unified approach. We compare our results with the state-of-the-art spatiotemporal SuStaIn method [21] by accessing the longitudinal stability and clinical correlations. The findings demonstrate our representation effectively captures robust pathology progression

patterns in longitudinal tau PET data. In the second experiment, we compare the longitudinal prediction accuracy with both statistic methods and an advanced deep learning method, where our method yields more accurate and interpretable results. The promising results demonstrate the great potential of using our topographical representation in enhancing longitudinal tau PET analysis for precise disease modeling and progression tracking.

2 Method

In this section, we firstly introduce the construction of topographical representation from Multiresolutional Reeb Graphs (MRGs). A topological similarity and a severity interleaving distance is then proposed for measuring the spatiotemporal pattern similarity and variations. A population-level graphical distribution is constructed according to the spatiotemporal relations, and a subtyping and staging integration system is proposed based on the connectivity of this distribution. Additional, a longitudinal prediction strategy is provided based on the population distributions.

2.1 Topographical Representation from Reeb Graph Analysis

The *Reeb graph* [13] is a topographic signature of real-valued functions and is widely used in geometric shape analysis [17][7], and hence is a natural choice for encoding the topographical information of cortical tau PET signals. We directly employed the method proposed for cortical surface structures [15][22] for the numerical calculation of Reeb graph of SUVR function f on surface $\mathcal{M}$. In essence, the Reeb graph describes the connected components of the level sets of a function. Because the topology only change at the critical points (minimum, saddle and maximum points), we firstly obtained all the critical points C, and their level contours. The connections between these critical points in the Reeb graph are obtained by applying region growing [15] on the mesh $\mathcal{M}$ and serve as the edges. The generated Reeb graph is represented as $R(f) = (C, E)$, where C is the nodes of the graph, corresponding to the critical points, and E is the set of edges, which are the partitions enclosed by two neighboring level contours.

The longitudinal topographical changes of tau pathology on cortical surface can be captured by the topology variations in the Reeb graphs. The emergence of the pathology corresponds to the appearance of salient components that gradual isolate from the background in Reeb graph (Fig. 1(b)), while its propagation can be represented by the expansion and further merging between connected components (Fig. 1(a)). Therefore, to seamless intergrate the static Reeb graph observation and the temporal progression of tau pathology, we extend the topographical representation into a Multiresolutional Reeb Graph (MRG) representation [7]. The basic idea of the MRG is to develop a series of Reeb graphs at multiple levels of detail, embedding temporal dynamics within spatial pattern characterization. A persistence-based simplification method [16] is taken

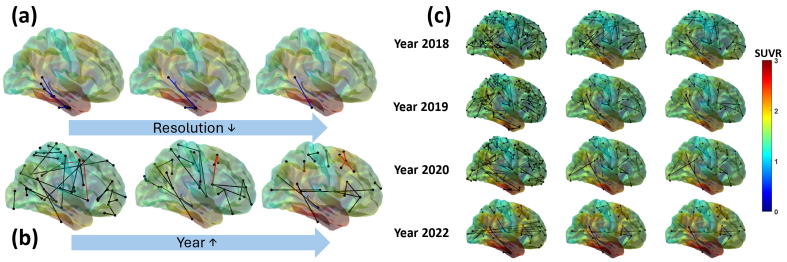

Fig. 1. Visualization of Multiresolutional Reeb Graphs (MRGs). (a) Pathology propagation is represented by edge expansion and fusion during graph simplification. (b) Pathology emergence is represented by edge formation across longitudinal scans, where red edges initially connected to the background become isolated as salient components. (c) Examples of MRGs for longitudinal scans of a same subject.

for producing the MRG. For an edge $E_k^n = (C_i^n, C_j^n)(f(C_i^n) < f(C_j^n))$ in the Reeb Graph $R^n(f) = (C, E^n)$ at resolution n, its persistence is defined as:

$$p(E_k^n) = A(E_k^n) \times f(C_j^n) \tag{1}$$

where $A(E_k^n)$ is the length of the edge E_k^n, usually calculated as the number of vertices included in this edge, and $f(C_j^n)$ is the peak SUVR value of this edge. To derive the Reeb graph at resolution $n+1$, we process nodes in decreasing order of peak SUVR based on the persistence threshold δ. We collapse edges E_k^n with $p(E_k^n) < \delta$, merge the node C_i^n (with a lower SUVR) into the node C_j^n (with a higher SUVR), and update the persistence for the new edge according to Equation 1. This simplification process continues until the threshold is reached, yielding a series of Reeb graphs at progressively coarser resolutions: $\{R^1 = (C^1, E^1), R^2 = (C^2, E^2), \ldots, R^N = (C^N, E^N)\}$ $(C^N \subset C^{N-1} \subset \ldots C^1)$. The MRG representation maintains topological consistency [7], such that (1) the parent-child relationships between nodes are consistent across levels; (2) iterative simplifications converge to the coarsest Reeb graph; (3) a Reeb graph of a certain level implicitly contains all the information of the coarser levels. The example of MRGs from a longitudinal subject is shown in Fig.1(c).

2.2 Spatiotemporal Similarity of Multiresolutional Reeb Graphs

We firstly develop a similarity metric for evaluating the tau pathology distribution similarity between static observations based on topology attributes of Reeb graph. Given the Reeb graph $R_x^m = (C_x^m, E_x^m)$ of a scan x at resolution m, the SUVR range of the edge $E_{x_i}^m$ is defined $r_{x_i^m} = \frac{[min(SUVR_{x_i^m}), max(SUVR_{x_i^m})]}{max(SUVR_x)}$ $(r_{x_i^m} \subset [0, 1])$. By integrating the spatial information of edges on the mesh $\mathcal{M}$ and their attributes of SUVR ranges, we could defined the local *topological similarity* $TS_{x_i^m, y_j^n}$ between two edges from two scans at individual resolutions as:

$$TS_{x_i^m, y_j^n} = \frac{A(E_{x_i^m} \bigcap E_{y_j^n})}{A(E_{x_i^m} \bigcup E_{y_j^n})} \cdot \frac{|r_{x_i^m} \bigcap r_{y_j^n}|}{|r_{x_i^m} \bigcup r_{y_j^n}|} \tag{2}$$

in which,A denotes the length of the edge. $r_{x_i^m}$ and $r_{y_j^n}$ are the SUVR ranges of the edges, and the operations between two SUVR ranges are defined as $r_{x_i^m} \bigcap r_{y_j^n} = \Big[\max(\inf(r_{x_i^m}), \inf(r_{y_j^n})), \min(\sup(r_{x_i^m}), \sup(r_{y_j^n}))\Big]$ and $r_{x_i^m} \bigcup r_{y_j^n} = \Big[\min(\inf(r_{x_i^m}), \inf(r_{y_j^n})), \max(\sup(r_{x_i^m}), \sup(r_{y_j^n}))\Big]$. This similarity measurement satisfies $0 \leq TS_{x_i^m, y_j^n} \leq TS_{x_i^m, x_i^m} = 1$.

To systematically characterize the global similarity between two Reeb graphs that integrating all edges, we propose a max-chain similarity that captures both the spatial distribution of pathology and the temporal progression coherence. This metric is inspired by the universal edit-distance of Reeb graph [1]. Given the edges of two scans at resolution m and n: $\{E_{x_1^m}, E_{x_2^m}, \ldots, E_{x_P^m}\}$ and $\{E_{y_1^n}, E_{y_2^n}, \ldots, E_{x_Q^n}\}$, where both sequences are sorted in decreasing orders of peak SUVR, the global max-chain similarity $TS_{x^m, y^n}$is defined as :

$$TS_{x^m, y^n} = \max_{S \subseteq \{(i,j)\}} \sum_{(i,j) \in S} TS_{x_i^m, y_j^n} \tag{3}$$

Here S is the non-crossing subset of the index pairs $\{(i, j)\}$, such that for any edge combinations (i, j) and (p, q), if we have $i \leq p$, we always have $j \leq q$.

To reduce the influence of Reeb graph complexity on similarity scaling, we normalize the similarity as $\bar{TS}_{x^m, y^n} = \frac{TS_{x^m, y^n}}{\sqrt{TS_{x^m, x^m}}\sqrt{TS_{y^n, y^n}}}$. This normalization ensures the similarity metric scale-invariant, enabling fair comparisons across graphs with different complexities.

Moreover, inspired by the interleaving distance of Reeb graphs [5], we define a *severity interleaving distance* between Reeb graph to measure the severity differences and temporal ordering between tau PET data as:

$$L_{x,y} = \sum_{(i,j) \in S} [(m_y^j - m_x^i) + \alpha(l_y^j - l_x^i)] \times A(E_{x_i^m}) \tag{4}$$

in which S is the max-chain non-crossing index pairs from Equation 3. m_x^i and m_y^j are the midpoints of the SUVR distributions of the edges, and l_x^i and l_y^j are the length of the SUVR ranges of the edges. The weight $\alpha = 0.5$ is taken in our experiments. This metric capture the global severity difference between two edges by quantifying the transformation cost between SUVR distributions.

To model the population distribution of tau PET data by integrating the spatiotemporal similarity of MRGs, we construct a directed graph, in which each scan is represented as a node and organized into layers corresponding to different disease stages. Within a stage, the edges connects the scans with similar spatial patterns and contains the edge attribute of the maximum topology similarity across resolutions. Across stages, edges link each scan to its longitudinal

follow-up or a cross-subject scan with high topological similarity and significant severity differences. This graph structure effectively captures both spatial pathology distribution and temporal progression within a unified framework.

2.3 Validation of Topographical Representation

We validate the topographical representation through a unified subtyping and staging task, evaluating whether the directed graph effectively captures spatiotemporal relationships in population. Additional, we perform longitudinal prediction on new data to further assess the efficacy of the spatiotemporal distributions.

Subtyping and Staging To achieve subtyping and staging while leveraging the structure of directed graph, we develop a multi-stage community detection algorithm based on the efficient Louvain method [2]. All the training data is initialized into multiple stages based on longitudinal time points. The community detection is applied within each stage by achieving:

$$\max(Q + \theta \sum_{x,y} R(x,y)\delta(c_x, c_y)) \tag{5}$$

where Q is the modularity of the graph. θ is the regularization weight, and $R(x,y) = 1$ when x and y are from the same subject, otherwise 0. c_x is the community assignment of vertex x, the δ-function $\delta(u,v)$ is 1 when $u = v$, otherwise 0.

The stage membership is further adjusted within each subtype according to:

$$\min(\sum_{x,y} \inf \times [q_x - q_y]^+ T(x,y) + [q_x - q_y]^+ L_{x,y}) \tag{6}$$

where q_x is the stage of scan x, $T(x,y) = 1$ if y is the longitudinal follow-up of x, $L_{x,y}$ is the severity interleaving distance between two scans, and $[t]^+ = 1$ if $t > 0$, otherwise 0.

The community detection and stage adjustment process is repeated until convergence or reaching the maximum iterations. This approach enables the simultaneous identification of subtypes and stages, ensuring both spatial coherence and longitudinal consistency in disease progression modeling.

Longitudinal Prediction Given the population-level distribution, we could predict the follow-up for a scan via group-wise spatiotemporal similarity and the temporal connections in the directed graph. For a scan x^t, we first identify the K most similar same-stage scans from the training data as $y_1^t, y_2^t, \ldots, y_K^t$. Their weights w_1, w_2, …, w_K are determined by normalizing topological similarities, ensuring $\sum_k(w_k) = 1$. Next, using the longitudinal relationships in the directed graph, we obtain their corresponding follow-up scans: $y_1^{t+1}, y_2^{t+1}, \ldots, y_K^{t+1}$. As a result, the estimation of $\tilde{x}^{t+1} = \sum_i w_i y_i^{t+1}$. This approach ensures the prediction preserves both spatial patterns and temporal progression. The illustration of the process is shown in Fig.2(a).

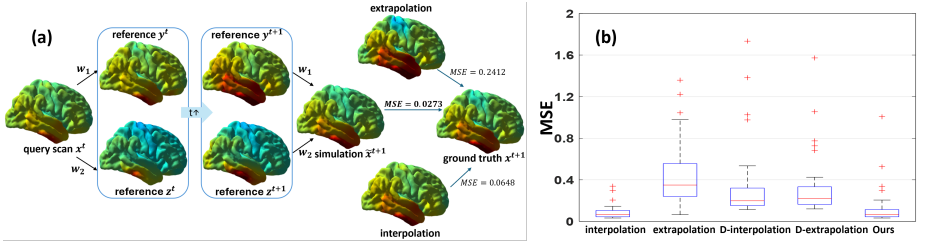

Fig. 2. Longitudinal prediction process and results.

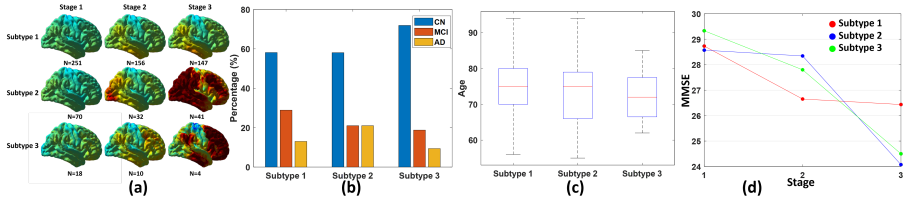

Fig. 3. (a) Average patterns in subtypes and stages. (b) Different subtypes exhibit different diagnostics distributions. (c) Different subtypes exhibit significant different($p < 0.05$) age distributions. (d) Different subtypes exhibit different cognitive decreasing rate across stages.

3 Experiments and Results

Totally 368 subjects with longitudinal tau PET scans from Alzheimer's Disease Neuroimaging Initiative (ADNI) dataset [11] are used in the experiments, including 285 subjects with 729 longitudinal scans for training and 83 subjects with 207 longitudinal scans for testing. All imaging data were preprocessed using the standard PETSurfer pipeline [6] for partial volume correction and intensity-normalization. The inferior cerebellar gray matter was used as the reference region to generate tau SUVR maps on cortical surfaces. In the current experiments, we use 6-level multi-resolution Reeb graph for all data as this level of complexity could sufficiently capture the majority of spatiotemporal features.

3.1 Longitudinal Subtyping and Staging

The subtypes and stages are derived from the connections among training data using the multi-stage community detection algorithm, which is elucidated in Section 2.3. To evaluate longitudinal stability, we compare our method with the popular spatiotemporal SuStaIn method [21]. The longitudinal stability is defined as the proportion of subjects classified into the same subtype across all time points. Directly using the mean SUVR within five ROIs (temporal, frontal, parietal, occipital, and medial temporal lobes) as biomarkers, the longitudinal stability of the SuStaIn method for defining three subtypes is only 68.07%. This

Method	Interpolation	Extrapolation	D-Interpolation	D-Extrapolation	Ours
MSE	0.0861	1.9585	0.3850	0.5412	**0.0529**

Table 1. Longitudinal prediction error.

instability is primarily due to the limited number of biomarkers and large samples of early-stage scans. While with a regularization weight of $\theta \geq 10^{-3}$, the longitudinal constrains in our method could ensure 100% longitudinal stability, demonstrating our approach effectively incorporates longitudinal data. This longitudinal constrains allow later scans with salient patterns to inform earlier scan memberships, which used to be challenging in subtyping. The superior longitudinal stability of our method indicates the proposed representation could successfully encode the spatiotemporal patterns, and the ability of modified community detection algorithm to leverage this dynamic representation structure.

The discovered pathology patterns are distinguished across subtypes, while keep a consistent phenotype within each subtype across stages (Fig.3(a)). We also perform a series of statistical analysis on biological and clinical measurements, with the results presented in Fig.3(b)(c)(d). The observed differences in diagnostic distribution, age distribution, and MMSE scores reveal the systematic difference across subtypes, and the different propagation speeds across stages. In Fig. 3(b), each subtype includes subjects across all diagnosis groups, indicating that the observed differences are not due to data imbalance.

3.2 Validation on Longitudinal Prediction

Using the longitudinal prediction approach as introduced in Section 2.3, we estimate the follow-up SUVR from one previous tau PET data as illustrated in Fig.2(a).

A learning-based disentanglement network [12] is used for comparison, which models the progression speeds in both normal aging and disease directions in the latent space z for a given pair of longitudinal scans. This enable two prediction strategies at time t: (1) D-Interpolation: estimate the speed with the given pairs at time $t-1$ and $t+1$, and reconstruct the scan at time t; (2) D-Extrapolation: estimate speed with the given pairs at time $t-2$ and $t-1$, and predict the scan at time t. Additionally, direct interpolation and extrapolation from SUVR maps are used as the baselines. Prediction error is measured by mean-square-error (MSE) as reported in Table. 1 and Fig.2(b). The deep learning based method and the direct extrapolation fail to estimate the vertex-wise individual progression rates due to the complexity caused by disease dynamics, resulting in suboptimal predictions. In contrast, our topographical representation effectively encodes the individual variability and the spatiotemporal progression of pathology, and graphical connections capture the group-wise similarity, our proposed longitudinal prediction approach reach the promising accuracy, outperforming than other methods.

4 Conclusion

In this paper, we propose a multiresolutional topographical representation for longitudinal tau PET data that integrating the spatial distribution and temporal propagation within a unified framework. A topology similarity and severity interleaving distance are then proposed based on the properties and structures of the representation for measuring the spatiotemporal similarity between scans. We validate and evaluate our approach on longitudinal ADNI data, demonstrating its effectiveness in subtyping, staging, and forecasting future tau accumulation.

Acknowledgments. This work was supported by the National Institute of Health (NIH) under grants R01EB022744, RF1AG077578, RF1AG064584, U19AG078109, and P30AG066530.

Disclosure of Interests. The authors have no competing interests to declare that are relevant to the content of this article.

References

1. Bauer, U., Landi, C., Mémoli, F.: The reeb graph edit distance is universal. Foundations of Computational Mathematics pp. 1–24 (2021)
2. Blondel, V.D., Guillaume, J.L., Lambiotte, R., Lefebvre, E.: Fast unfolding of communities in large networks. Journal of statistical mechanics: theory and experiment **2008**(10), P10008 (2008)
3. Bollack, A., Pemberton, H.G., Collij, L.E., Markiewicz, P., Cash, D.M., Farrar, G., Barkhof, F., on behalf on the AMYPAD consortium: Longitudinal amyloid and tau pet imaging in alzheimer's disease: a systematic review of methodologies and factors affecting quantification. Alzheimer's & Dementia **19**(11), 5232–5252 (2023)
4. Braak, H., Braak, E.: Neuropathological stageing of alzheimer-related changes. Acta neuropathologica **82**(4), 239–259 (1991)
5. De Silva, V., Munch, E., Patel, A.: Categorified reeb graphs. Discrete & Computational Geometry **55**(4), 854–906 (2016)
6. Greve, D.N., Svarer, C., Fisher, P.M., Feng, L., Hansen, A.E., Baare, W., Rosen, B., Fischl, B., Knudsen, G.M.: Cortical surface-based analysis reduces bias and variance in kinetic modeling of brain pet data. Neuroimage **92**, 225–236 (2014)
7. Hilaga, M., Shinagawa, Y., Kohmura, T., Kunii, T.L.: Topology matching for fully automatic similarity estimation of 3d shapes. In: Proceedings of the 28th annual conference on Computer graphics and interactive techniques. pp. 203–212 (2001)
8. Jack Jr, C.R., Bennett, D.A., Blennow, K., Carrillo, M.C., Dunn, B., Haeberlein, S.B., Holtzman, D.M., Jagust, W., Jessen, F., Karlawish, J., et al.: Nia-aa research framework: toward a biological definition of alzheimer's disease. Alzheimer's & dementia **14**(4), 535–562 (2018)
9. Jeon, S., Kang, J.M., Seo, S., Jeong, H.J., Funck, T., Lee, S.Y., Park, K.H., Lee, Y.B., Yeon, B.K., Ido, T., et al.: Topographical heterogeneity of alzheimer's disease based on mr imaging, tau pet, and amyloid pet. Frontiers in aging neuroscience **11**, 211 (2019)

10. Leuzy, A., Raket, L.L., Villemagne, V.L., Klein, G., Tonietto, M., Olafson, E., Baker, S., Saad, Z.S., Bullich, S., Lopresti, B., et al.: Harmonizing tau positron emission tomography in alzheimer's disease: The centaur scale and the joint propagation model. Alzheimer's & Dementia **20**(9), 5833–5848 (2024)
11. Mueller, S.G., Weiner, M.W., Thal, L.J., Petersen, R.C., Jack, C., Jagust, W., Trojanowski, J.Q., Toga, A.W., Beckett, L.: The alzheimer's disease neuroimaging initiative. Neuroimaging Clinics **15**(4), 869–877 (2005)
12. Ouyang, J., Zhao, Q., Adeli, E., Zaharchuk, G., Pohl, K.M.: Disentangling normal aging from severity of disease via weak supervision on longitudinal mri. IEEE transactions on medical imaging **41**(10), 2558–2569 (2022)
13. Reeb, G.: Sur les points singuliers d'une forme de pfaff completement integrable ou d'une fonction numerique [on the singular points of a completely integrable pfaff form or of a numerical function]. Comptes Rendus Acad. Sciences Paris **222**, 847–849 (1946)
14. Schwarz, A.J., Shcherbinin, S., Slieker, L.J., Risacher, S.L., Charil, A., Irizarry, M.C., Fleisher, A.S., Southekal, S., Joshi, A.D., Devous Sr, M.D., et al.: Topographic staging of tau positron emission tomography images. Alzheimer's & Dementia: Diagnosis, Assessment & Disease Monitoring **10**, 221–231 (2018)
15. Shi, Y., Lai, R., Toga, A.W.: Cortical surface reconstruction via unified Reeb analysis of geometric and topological outliers in magnetic resonance images. IEEE Transactions on Medical Imaging **32**(3), 511–530 (2012)
16. Shi, Y., Li, J., Toga, A.W.: Persistent Reeb graph matching for fast brain search. In: International Workshop on Machine Learning in Medical Imaging. pp. 306–313. Springer (2014)
17. Shinagawa, Y., Kunii, T.L.: Constructing a reeb graph automatically from cross sections. IEEE Computer Graphics and Applications **11**(06), 44–51 (1991)
18. Villemagne, V.L., Doré, V., Burnham, S.C., Masters, C.L., Rowe, C.C.: Imaging tau and amyloid-β proteinopathies in alzheimer disease and other conditions. Nature Reviews Neurology **14**(4), 225–236 (2018)
19. Vogel, J.W., Iturria-Medina, Y., Strandberg, O.T., Smith, R., Levitis, E., Evans, A.C., Hansson, O.: Spread of pathological tau proteins through communicating neurons in human alzheimer's disease. Nature communications **11**(1), 2612 (2020)
20. Vogel, J.W., Young, A.L., Oxtoby, N.P., Smith, R., Ossenkoppele, R., Strandberg, O.T., La Joie, R., Aksman, L.M., Grothe, M.J., Iturria-Medina, Y., et al.: Four distinct trajectories of tau deposition identified in alzheimer's disease. Nature medicine **27**(5), 871–881 (2021)
21. Young, A.L., Marinescu, R.V., Oxtoby, N.P., Bocchetta, M., Yong, K., Firth, N.C., Cash, D.M., Thomas, D.L., Dick, K.M., Cardoso, J., et al.: Uncovering the heterogeneity and temporal complexity of neurodegenerative diseases with subtype and stage inference. Nature communications **9**(1), 4273 (2018)
22. Yue, J., Shi, Y.: Uncovering heterogeneity in Alzheimer's disease from graphical modeling of the tau spatiotemporal topography. In: International Conference on Medical Image Computing and Computer-Assisted Intervention. pp. 262–271. Springer (2023)